Characterization of the boron profile and coordination in altered glass layers by EEL spectroscopy

H. Aréna, Renaud Podor, H.-P. Brau, J. Nelayah, N. Godon, M. Cabié, E. Garcès, C. Mansas, D. Rébiscoul

Characterization of the boron profile and coordination in altered glass layers by EEL spectroscopy.

H. Aréna[1], R. Podor[2], H.-P. Brau[2], J. Nelayah[3], N. Godon[1], M. Cabie[4], E. Garcès[1], C. Mansas[1], D. Rébiscoul[2]

[1] CEA, DES, ISEC, DE2D, Univ Montpellier, Marcoule, France
[2] ICSM, Univ Montpellier, CNRS, CEA, ENSCM, Bagnols-sur-Cèze, France
[3] Université de Paris, Laboratoire Matériaux et Phénomènes Quantiques, CNRS, 75013 Paris, France
[4] Aix-Marseille Université, CNRS, Centrale Marseille, FSCM, CP2M, Marseille, France

Corresponding author: helenearena@orange.fr

Keywords: EELS, alteration layer, glass, boron profile, interface, boron coordination

Abstract

Electron energy-loss spectroscopy was used to characterize the boron profile and its coordination (B^{III} and B^{IV}), along the complex alteration layer of glass samples altered for 511 days at 50°C in solution containing $FeCl_2$, $MgCl_2$ and/or $CaCl_2$. To reach this goal, the impact of both TEM operating conditions and sample preparation on the determination of the boron coordination was first studied using mineralogical and pristine glasses reference samples. Then, the boron concentration profiles were characterized in the glass alteration layer. These profiles were found to be S-shaped with a thickness around forty nanometers. The proportion of B^{III} was found to decrease with the boron total concentration (from the pristine glass to the gel layer), which suggests a higher bonding strength for B^{IV} bonds than that of B^{III} bonds under the alteration conditions. These findings are of tremendous interest to advance further in the understanding of glass alteration mechanisms.

Introduction

Water-rock interactions are of great interest in several fields of research like earth science, environment, material science and also nuclear glasses management. Rock alteration in contact with water or in wet environments leads to surface changes such as the formation of an alteration layer. This is the case of the borosilicate nuclear glasses in which high level radioactive wastes are vitrified. In the French concept of nuclear waste

management, the nuclear glasses are intended for long-term disposal in a geological repository. Glass alteration by underground water is the main risk of radioactive elements release in the environment. It involves several processes and leads to the formation of a stratified alteration layer. From the pristine glass to the solution, this layer is composed by i) a hydrated, desalkalinized and partly boron depleted glass zone, ii) a gel layer, and above iii) secondary silicates like smectites may precipitate, forming a rough and nanocrystalline layer. The hydrated glass layer is very thin and located at the interface between the gel layer and the pristine glass. The gel layer is a nanoporous hydrated silica-based material formed by condensation of the dissolved species in solution, such as Si, Al and Ca, which acts as a protective barrier slowing down water penetration (Gin, Ryan et al. 2013, Rébiscoul, Cambedouzou et al. 2015). The protective properties of the gel are related to its thickness and composition, which can vary depending on the alteration conditions (Rebiscoul, Van der Lee et al. 2004, Cailleteau, Angeli et al. 2008). Glass alteration is usually monitored by the boron release in solution because this element is fully present in pristine glass, partly present in the hydrated glass layer, and absent from the gel and the secondary phases. One way to evaluate and compare the diffusion properties of alteration layers is to determine the boron profile in the hydrated and desalkalinized glass zone located at the gel / pristine glass interface (Gin, Guittonneau et al. 2011).

Several characterization techniques have already been tested and compared to determine the boron profile in glass alteration layers. The apparent thickness of the boron profile was found to decrease when the spatial resolution of the technique increased (Gin, Guittonneau et al. 2011, Moutanabbir, Isheim et al. 2011, Gin, Ryan et al. 2013, Wang, Liu et al. 2016, Gin, Jollivet et al. 2017). Among them, Time of Flight Secondary Ion Mass Spectroscopy (ToF-SIMS) is often used because it is quite easy to perform, but the surface irregularities of the sample can induce mixing zones and widen the apparent boron concentration profile. This technique should therefore be reserved to samples with a planar altered surface (without secondary phases). Energy-Filtered Transmission Electron Microscopy (EFTEM) and Atom-Probe Tomography (APT) showed interesting results for both complex and simple glasses (Gin, Ryan et al. 2013, Gin, Jollivet et al. 2017), and enabled to monitor the effects of irradiation on the thickness of the boron concentration profile (Mougnaud, Tribet et al. 2018). APT seems

to be the most accurate and reliable technique as it offers the possibility to determine the position of elements (light and heavy elements) with a subnanometer resolution. However, this last technique requires a specific preparation relatively difficult to perform for complex materials such as glass / gel layers, and the method used for the reconstruction of the analyzed volume of the sample suffers from uncertainties (Wang, Liu et al. 2016). Finally, all these techniques can be used to determine the thickness of the boron concentration profile in altered glasses, but none of them enables the assessment of the boron coordination along this profile. In glasses structure, the boron coordination may vary depending on the elements present in its composition and this information could improve the current understanding of glass alteration processes.

In this study, we have used spatially-resolved electron energy loss spectroscopy (EELS) coupled with TEM analyses to study the boron profile at the pristine glass / gel interface, in terms of shape, thickness, as well as local coordination. Thanks to its high spatial resolution (down to 1 nm) and detection sensitivity (0.1 to 1 at.%), EELS is a powerful technique which has been successfully used to study boron local enrichments in materials like nanocrystalline diamond films (Wurzinger, Pongratz et al. 1997, Dubrovinskaia, Wirth et al. 2008, Lu, Turner et al. 2012) and carbon nanotubes (Shindou, Hamamura et al. 2010). Thanks to its high sensitivity, EELS has enabled the detection of local boron concentrations of about 1 at% in solar cells and nanocrystalline diamond films (Turner, Lu et al. 2012, Duchamp, Boothroyd et al. 2013, Turner, Lu et al. 2016). Moreover, Van Aken *et al.* have even been able to study boron profiles of a few tens of nanometers at the interface between two layers of a solar cell (Van Aken, Duchamp et al. 2012). EELS has been used to determine the boron concentrations and local environments in minerals (Garvie, Craven et al. 1995). In glass samples, EEL spectroscopy has been mainly used to determine the boron coordination and the possible changes due to irradiation exposure (Jiang and Silcox 2004, Yang, Saghi et al. 2007, Bingham, Yang et al. 2008, Yang, Möbus et al. 2009, Cheng, Yang et al. 2015) but never used to characterize the boron coordination in the boron concentration profile in glass alteration layer.

Herein, we report and discuss, for the first time, the use of EELS at the B-K edge to determine the boron concentration profile and coordination-specific boron site occupancies across the gel / pristine glass interface in altered glasses. To reach this goal, we have first studied the impact of the TEM operating conditions and of the sample preparation on the determination of the boron coordination. Second, this technique was applied on three samples of glass altered during 511 days in solutions containing $FeCl_2$, Mg Cl_2 and/or $CaCl_2$ (Aréna, Rébiscoul et al. 2018). These samples were selected because previous studies have shown that iron and magnesium yield to an increase of glass alteration and more particularly to the formation of secondary phases (Fleury, Godon et al. 2013, Michelin, Burger et al. 2013, Dillmann, Gin et al. 2016, Aréna, Godon et al. 2017, Aréna, Rébiscoul et al. 2018) whereas calcium, integrated into the gel layer makes it more protective (Chave, Frugier et al. 2011, Mercado-Depierre, Angeli et al. 2013, Aréna, Rébiscoul et al. 2019). These changes in alteration rates are related to the modification of the altered layers composition, morphology and physical properties. At a nanometer scale, the thickness of the boron concentration profile is modified but no information is available about the boron local environment in the hydrated glass zone between the gel and the pristine glass. Finally, taking into account the limits and uncertainties of the method, the results concerning the evolution of the boron coordinence across the gel / pristine glass interface are linked to glass alteration mechanisms.

1 Materials and methods

1.1 Samples

Mineralogical samples of vonsenite and rhodizite, simple GB0.5 glass (Mansas, Delaye et al. 2017) and the International Simple Glass (ISG) (Gin, Abdelouas et al. 2013) were used as reference materials (Table 1). Rhodizite and GB0.5 glass were prepared by grinding with a mortar and pestle, producing a suspension in acetone and pipetted it onto holey carbon thin film grids. For electron microscopy, ISG glass thin foils were prepared using a dual beam FIB/SEM instrument (FEI Helios 600 Nanolab) allowing in-situ FIB-liftout (Giannuzzi and Stevie 1999). To prevent bending of the lamella once the foil is approaching its final thickness the lamella was fixed in the middle of the M shaped pin of a copper grid. In addition, only a small area of the whole lamella (5 µm long by 3 µm height) was thinned to electron transparency (around 100 nm thick).

Table 1: References, composition, sample preparation of the references samples used in this study.

Sample name	**Vonsenite**	**Rhodizite**	**GB0.5**	**ISG**
Sample type	Mineralogical	Mineralogical	Pristine glass	Pristine glass
Composition	$Fe^{2+}2Fe^{3+}(BO_3)O_2$	$M_{0.9}Al_4Be_{4.55}B_{11.35}O_{28}$ (M = mixture of alkali metals)	SiO_2 (62.9 mol%) B_2O_3 (15.3 mol%) Na_2O (12 mol%) Al_2O_3 (4.2 mol%) CaO (5.6 mol%)	SiO_2 (44.3 mol%) B_2O_3 (35.4 mol%) Na_2O (11.8 mol%) Al_2O_3 (4.9 mol%) CaO (2.8 mol%) ZrO_2 (0.8 mol%)
B^{III} expected percentage (%)	100 (Raman spectroscopy) (Ray L. Frost, Ricardo Scholz et al. 2013)	0 (NMR) (Pring, Din et al. 1986)	44 (NMR) (Mansas, Delaye et al. 2017)	51 (NMR) (Gin, Abdelouas et al. 2013)
Preparation	grinded powder on holey carbon films			FIB thin foil

ISG glass monoliths were placed into glass powders and altered in aqueous solution during 511 days at 50°C, with a surface of glass to solution volume ratio (S/V) of 200 cm^{-1}. The experiments were conducted in nitrogen glove box and three different electrolyte solutions containing $FeCl_2$ at 10 $mmol.L^{-1}$ (experiment F), a mixture of $MgCl_2$ and $FeCl_2$ at 5 $mmol.L^{-1}$ each (experiment MF), or a mixture of $CaCl_2$ and $FeCl_2$ at 5 $mmol.L^{-1}$ each (experiment CF) were used. For more details on the alteration procedure, please refer to the following papers devoted to glass alteration (Aréna, Godon et al. 2016, Aréna, Godon et al. 2017, Aréna, Rébiscoul et al. 2018). For EELS analyses, high resolution TEM (HR-TEM) and high-angle annular dark field (HAADF-STEM) imaging of these samples, thin foils were prepared from altered glass monoliths, as previously described, by FIB.

1.2 Experimental conditions

Transmission electron microscopy (TEM) studies were undertaken with a JEM ARM 200F (JEOL) transmission electron microscope equipped with a cold-field emission gun and a CEOS aberration corrector of the objective lens (Ricolleau, Nelayah et al. 2013). A particular attention was paid on the choice of the observation conditions in order to limit beam damage of the samples. Boron materials are highly susceptible to electron-beam-induced damage (Sauer, Brydson et al. 1993). The microscope was thus operated

at an accelerating voltage of 80 kV in the present study since at 200 kV irreversible and intensive mass loss was observed during TEM observation. The spot size was below 1 nm in size. Aberration-corrected high-resolution transmission electron microscopy (HR-TEM) images were acquired in TEM mode. High-angle annular dark-field imaging, spatially-resolved electron energy loss spectroscopy (EELS) and energy dispersive X-ray spectroscopy (EDS) were performed with the microscope operated in scanning mode (STEM mode) with probe size setting set at "5C". EEL spectra were acquired using a Gatan Quantum ER imaging filter fitted with a fast CCD camera operating in high quality mode at a dispersion of 0.05 eV/channel (energy resolution). The convergence and collection angles for EELS measurements were fixed at 32 mrad and 50 mrad respectively. Under these illumination conditions, the electron probe current was about 0.025 nA and the electron dose was about 4×10^{-11} A nm^{-2}. Spatially-resolved EELS spectra over two-dimensional regions of the sample were acquired sequentially in space in the spectrum-image mode. To further limit sample damage during EELS data acquisition, sub-pixel scanning (16×16) was activated during spectrum-imaging acquisition.

1.3 Data treatment

Energy instabilities during EELS acquisition were corrected by measuring the energy shift of the B^{III} main peak or of the B^{IV} main peak. After energy drift correction, the background was fitted and subtracted using a power law function. ImageJ software (Schneider, Rasband et al. 2012) associated with the CSI module (Hovden, Cueva et al. 2013) was used to perform EEL spectra data processing including background subtraction at the B-K edge. When necessary, the spectral base line was also corrected after background subtraction. Finally, to facilitate the comparison between the samples, the intensity was integrated over the 192.2 to 206.8 eV range and normalized data were used.

1.4 Determination of the B^{III} percentage

Depending on boron coordination, the EEL spectra at the B K-edge are characterized by several fine features (Figure 1). Trigonal B^{III} edge like in vonsenite shows a sharp peak at 193.8 eV (peak A), followed by two broader peaks around 199 eV and 204 eV (peak C). Tetragonal B^{IV} edge like in rhodizite presents a sharp peak at 198.6 eV (peak B) and a

shoulder around 204 eV. The differences between these fingerprints can be explained by molecular orbital theory as reported in (Sauer, Brydson et al. 1993).

Berger *et al*. have developed a procedure to determine the fraction of sp2-bonded carbon atoms contributing to the C ls spectrum of amorphous diamond-like carbon films (Berger and McKenzie 1988) and Sauer *et al.* adapted it to estimate the proportion of B^{III} in several minerals (Sauer, Brydson et al. 1993). According to Equation 1, the R ratio between *J(A)*, the integrated intensity of peak A (from 192.55 to 195.05 eV) and $J(\Delta E)$, and the integrated intensity of a 14.6 eV window (from 192.4 to 207 eV), is calculated for the sample and compared with the corresponding R ratio obtained for a reference material containing 100 % of B^{III}. This method was used for several minerals in (Garvie, Craven et al. 1995). The relative error in the estimation of the B^{III} proportion ranged from 5 to 30 %. Error calculations are reported in details in SI 1.

$$\% B^{III} = \frac{R_{sample}}{R_{reference}} = \frac{\left[\frac{J(A)}{J(\Delta E)}\right]_{sample}}{\left[\frac{J(A)}{J(\Delta E)}\right]_{reference}} \times 100 \qquad (1)$$

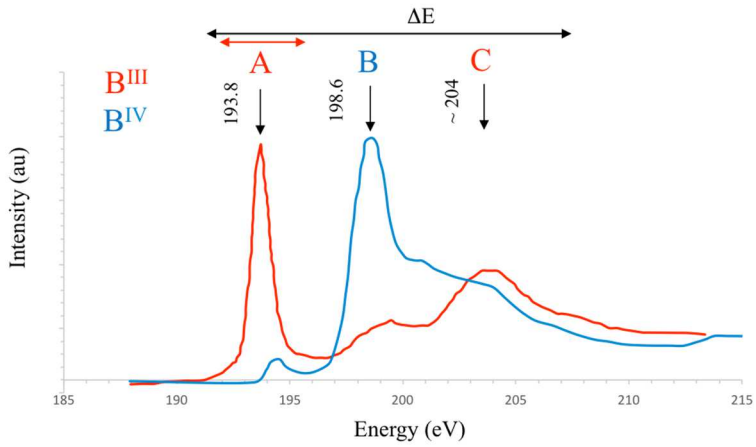

Figure 1: EEL spectra at the B-K edge in vonsenite (planar-trigonal B^{III} coordination_red line) and rhodizite (tetrahedral B^{IV} coordination_blue line) from (Sauer, Brydson et al. 1993). Illustration of Sauer procedure using two integration windows (A and ΔE) to determine the % B^{III}.

We initially tried to use vonsenite which is known to contain only B^{III} units (Ray L. Frost, Ricardo Scholz et al. 2013), to acquire a 100 % B^{III} reference spectrum but our sample was not pure enough to provide useful data. As reported in the literature, the coordination of boron evolves from B^{IV} to B^{III} under electron beam exposure (Sauer, Brydson et al. 1993, Yang, Möbus et al. 2009). This transformation was observed for

rhodizite and GB0.5 glass samples. After a sufficient exposure time, the EEL spectrum of rhodizite sample showed only the B^{III} feature without further evolution. Therefore, an average spectrum calculated from 25 spectra of irradiated rhodizite was finally used as a reference for 100 % of B^{III}.

1.5 Determination of the boron profile

The procedure used to obtain the boron profile in the alteration layer is described on Figure 2. Firstly, areas of interest ranging from 10 450 to 4 500 nm^2 were selected and divided into pixels with a spatial sampling between 4 and 25 nm^2 (Figure 2-c, step 1). Secondly, as stated before, EEL spectra at the B-K edge were acquired for each pixel (step 2). It should be noted that the EELS information measured in each pixel corresponds to the average signal integrated over the sample volume beneath the pixel. After background removal, the EEL spectra were integrated from 191.5 eV to 211.5 eV (to take into account both trigonal and tetragonal boron contributions) to generate a boron intensity map, showing the evolution of the boron concentrations between the pristine glass (white) and the gel (black) (Figure 2-d). Thirdly, each horizontal set of pixels lead to a boron intensity profile across the pristine glass / gel interface with a lateral resolution ranging from 2 to 5 nm (Figure 2-e, step 3). Finally, the boron concentration profiles were averaged on all pixel lines (Figure 2-f, step 4 - red curve) and fitted by a Boltzmann type function to enable their comparison and the determination of their thicknesses (Figure 2-f, step 4 black curve - SI 2).

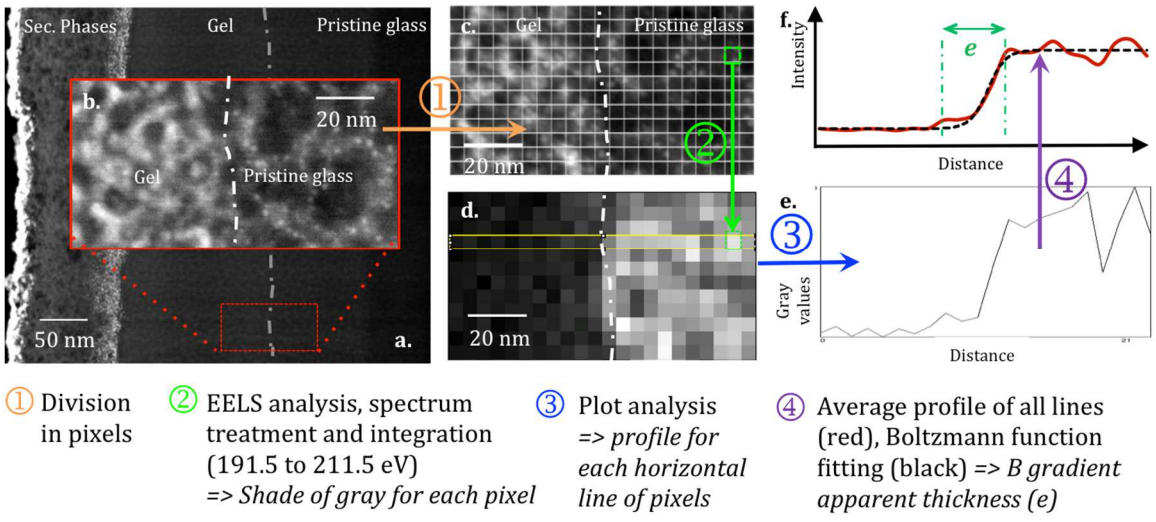

Figure 2: Procedure used to extract the boron profile from EELS analyses: a) and b) TEM observations of the gel / pristine glass interface, c) division of the analyzed area into pixels, d) intensity map obtained after integration, e) and f) resulting boron concentration profiles. For all samples, complete data is given in SI 2.

2 Results and Discussion

2.1 Selection of the optimal conditions: Reference samples

Rhodizite mineral

Rhodizite EEL spectra (Figure 3-a) were acquired after different times of exposure to the electron beam. From the EEL spectra, the R ratio and the percentage of B^{III} units (% B^{III}) were plotted as a function of the exposure time (Figure 3-b).

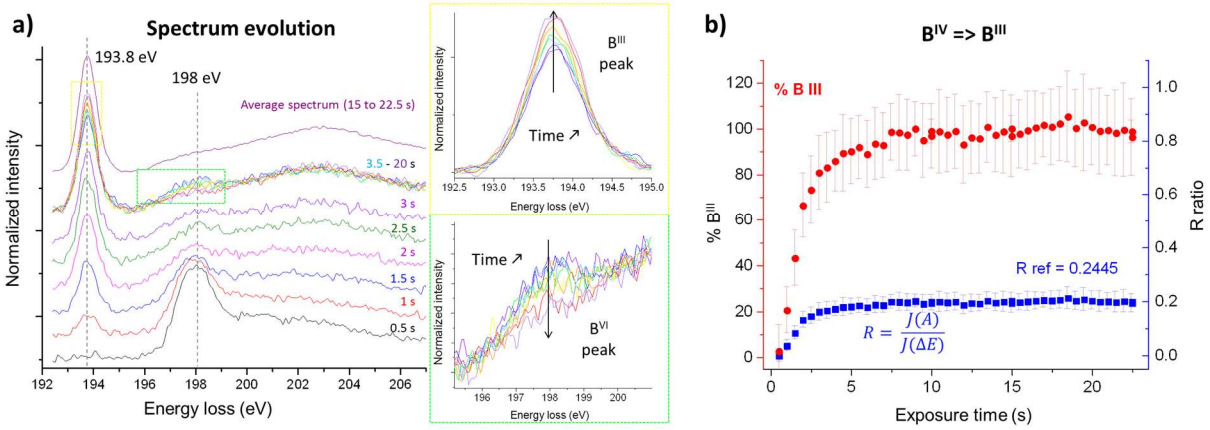

Figure 3 : a) Evolutions of EEL spectrum of rhodizite. b) Evolutions of the percentage of B^{III} units as a function of the irradiation time.

The first spectra of rhodizite showed the characteristic feature of B^{IV}: no peak around 193.8 eV, a sharp peak at 198 eV and a shoulder around 203 eV. The % B^{III} was evaluated to 2.6 ± 11 % which is low but not null. As rhodizite contains only B^{IV} units (Pring, Din et al. 1986), this non null value shows that boron coordination evolves quickly under the electron beam in this mineral, despite the soft acquisition conditions and the short exposure time (0.1 s). As the exposure time increased, the intensity of the main peak of B^{IV} (198.1 eV) decreased while the intensity of the characteristic peak of B^{III} increased (193.8 eV). Even though the error bars are quite high, a clear trend can be noted: the R ratio and the proportion of B^{III} increased sharply during the first 0.5 s until almost 80 % of B^{III} then the increase slowed down (Figure 3-b). Complete transformation of B^{IV} into B^{III} was reached after about 7.5 s of exposure.

From these results, it appears that the damages induced by electron beam exposure occur quickly, and strongly modify boron coordination. This kind of damages has

already been reported in the literature for various alkali borosilicate glasses and minerals (Sauer, Brydson et al. 1993, Jiang and Silcox 2004, Yang, Mobus et al. 2006, Yang, Möbus et al. 2006, Yang, Möbus et al. 2009). In addition, when the exposure time was too long, the formation of holes was observed on the samples (SI 3).

GB0.5 glass grains

In order to determine the homogeneity of the sample preparation and the reliability of the method, EEL B-K edge spectra were acquired on GB0.5 glass grains deposited on a Cu holder. From NMR analysis, this GB0.5 glass is expected to have 44 % (Mansas, Delaye et al. 2017) of B^{III}. Several locations were probed to record EEL spectra and calculate the B coordination (Figure 4).

The results show that the acquisition of useable spectra on such materials is complicated. Only 3 sites out of the 10 locations probed gave usable EEL spectra, which can be linked to the variation of the sample thickness. Indeed, when the probed area was too thick the fine-structure was hidden by a high background intensity, and when the area was thin enough to minimize the intensity of the background, the quantity of B was too low to be detected. In addition, B tended to migrate out of the sample under beam exposure, leading to a decrease in the signal-to-noise ratio. This highlights that the sample preparation used, i. e. glass grinding and deposition, was not optimal to obtain the needed compromise between sample thickness, background intensity and boron concentration.

Moreover, the % B^{III} determined from the first spectrum (before electron beam exposure) of the three usable sites, varied with the area probed. Despite their close-range locations (13 and 24 nm – Figure 4-c), the three probed sites gave various results. Site 1 and site 3 framed the NMR value (33 ± 13 % and 57 ± 21 %, respectively), while site 2 gave a much higher value (82 ± 20 %). These results show that EELS is a local technique (spot size below 1 nm), impacted by local variations while NMR is a global technique which probes the bulk. Indeed, glass structure is complex, despite an ordered organization at long-range, it can be disordered at short-range with the presence of clusters which could impact the local boron coordination. In addition, under the electron beam, phase separation may occur in borosilicate glasses (Denatale and Howitt 1984, K. Sun, L.M. Wang et al. 2004). This phenomenon would favor local changes in B environment, and thereby in its coordination.

Finally, as for rhodizite, the spectra of the three sites evolved under electron beam exposure, toward an increase in the B^{III} proportion. However, for sites 1 and 3 of the GB0.5 glass, the maximum of % B^{III} reached was about 90 % and the transformation was a bit slower than for rhodizite (7 seconds to go from 35.6 % to 90 % B^{III} and 7.5 s to go from 2.6 to 100 % B^{III}, respectively).

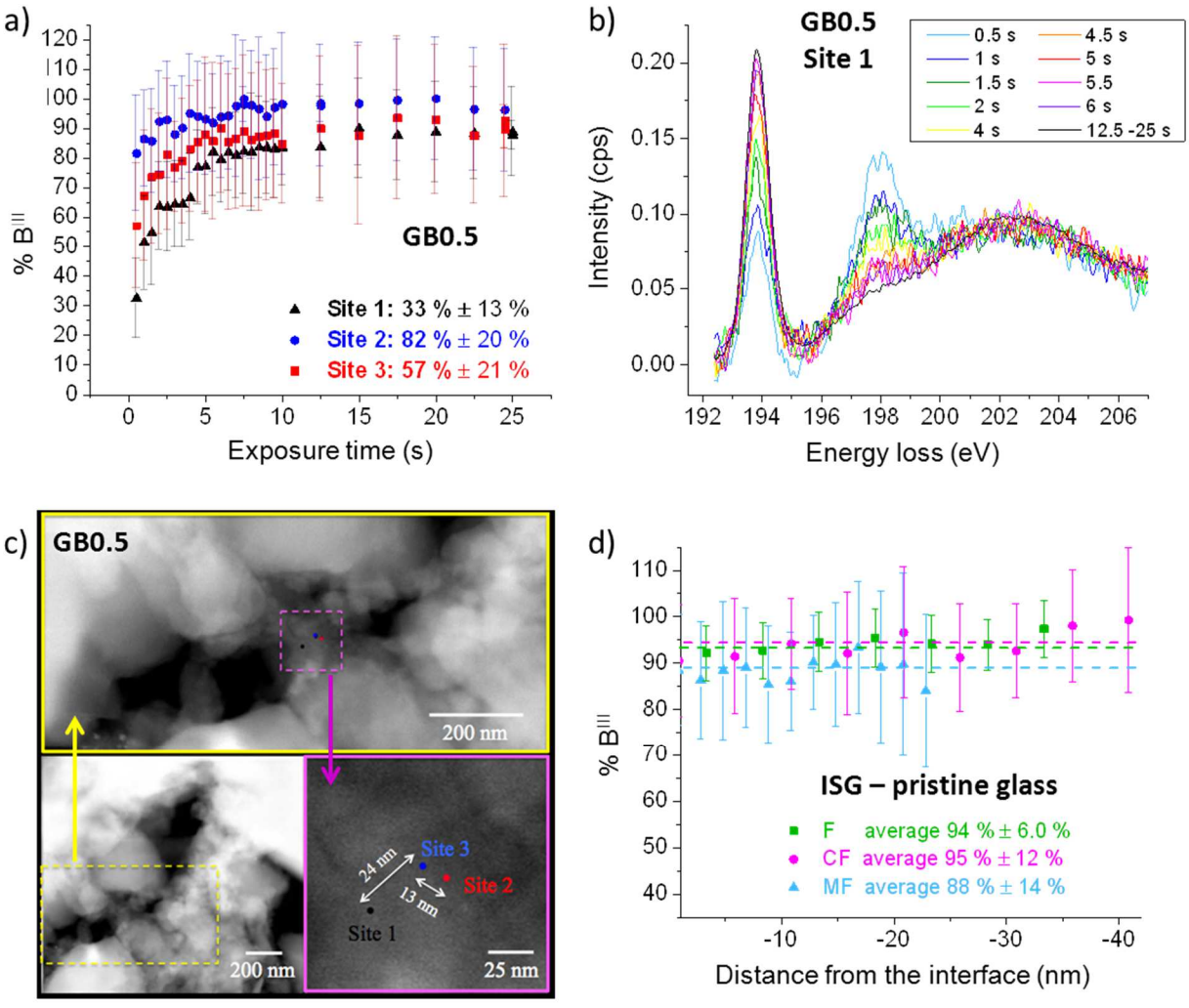

Figure 4 : a) Evolutions of the percentage of B^{III} as a function of the exposure time under the electron beam for several sites of GB 0.5 sample, b) EELS B-K edge spectra of GB0.5 site 1, c) STEM DF images of the three probed sites, and d) Evolution of the percentage of B^{III} in the pristine glass area, as a function of the distance from the interface in ISG thin foils.

The results obtained for GB0.5 glass showed that this method is very sensitive to the sub-nanometer local variations in B coordination, which may be expected in materials such as glasses. In addition, the sample preparation is of high importance since it impacts the quality and the usability of the recorded EEL spectra. Thus, in order to

improve the sample preparation, control their thicknesses and study the local B coordination in another glass, ISG thin foils, of about 100 nm thick, were prepared.

Pristine ISG thin foils

FIB thin foils were prepared on ISG monoliths altered in electrolytes containing $FeCl_2$ alone and with $MgCl_2$ or $CaCl_2$. TEM HAADF images showed the altered layers and enabled the localization of the pristine glass area (Figure 5). For each sample, at least 7 areas in pristine glass were probed with a spatial step of 2 to 5 nm (Figure 4-d).

For all samples, the obtained % B^{III} values in pristine glass were quite dispersed from one location to another, even with a nanometric spatial step. However, this dispersion was lower than that of GB0.5 glass, which could be explained by two hypotheses: (i) Thanks to its controlled and homogenous thickness, the FIB thin foil preparation is more adapted to our samples. (ii) GB0.5 glass structure is less homogenous than that of ISG. According to the literature, the sensitivity of borosilicate glasses to electron damage appears to be related to their composition, and especially to the nature and the proportion of alkali acting as network modifiers (Yang, Möbus et al. 2006, Yang, Möbus et al. 2009). The proportion of alkali is higher in GB0.5 glass than in ISG, and the amount of the negative structures to be compensated ($[AlO_4]^-$ and $[ZrO_6]^{2-}$) is lower. Therefore, GB0.5 glass is probably more sensitive to electron beam damages than ISG, which would favor local phase separation and B coordination change. Unfortunately, the evolutions of EEL spectra as a function of time were not acquired for ISG, which would have enabled a better assessment of this hypothesis.

The average values of % B^{III} were estimated at 94 ± 6.0 %, 95± 12 % and 88 ± 14 % for samples F, CF and MF, respectively. The % B^{III} in the bulk of pristine ISG glass has been measured to 51.6 ± 5, by NMR of boron in (Mendoza, Peuget et al. 2014). The values found here by the interpretation of EEL spectra were much higher than the one found by NMR. Several explanations can be suggested. (i) NMR is a global technique which probes the bulk sample while EELS is more local. The remaining dispersion of the values from one area to another emphasizes this point and suggests that the local coordination of boron differs from the bulk one. (ii) Despite the soft operating TEM conditions applied

(80 kV and limited exposure time during EELS acquisition), the B^{III}/B^{IV} coordination could have already evolved due to electron beam exposure, by the time of the EELS acquisition (0.5 to 2 s). (iii) It may be also suggested that the FIB preparation could also induce the partial transformation of some B^{IV} groups into B^{III} groups due to ionic beam damages.

Despite high error bars and the possible lack of accuracy on the absolute B values due to the recording conditions, the results acquired on reference materials enabled the validation of the method, and the determination of the optimized acquisition conditions. The sample preparation as FIB thin foil seems to improve the quality of the EEL spectra and to reduce the dispersion of the calculated B^{III} percentage values. In addition, the materials are sensitive to electron beam damages, therefore the calculated B^{III} percentage may be slightly overestimated. Nevertheless, the spectra acquired at short time conditions are expected to be representative of the non-irradiated materials. Moreover, despite its limitations, this method enables the determination of changes in the boron coordinence at the nanometric scale, making it suitable for the study of layered materials with thin interfaces like altered glasses.

2.2 Complex samples: altered glass thin foils

As explained in the introduction, several information only accessible by HR-TEM, HAADF-STEM and EEL B-K spectroscopy are of paramount importance to improve the glass alteration understanding. These techniques enabled the localization of the gel / pristine glass interface, the determination of the boron concentration profile shape and thickness, and the evolution of the boron coordination across this interface.

Localization of the gel / pristine glass interface

The three thin foils have been characterized by HR-TEM and HAADF-STEM (Figure 5 – SI 4 and 5). Several sublayers were observable in the alteration layer: the secondary phases, platinum particles deposited during the thin foil preparation, a gel and the pristine glass. Observations at very high magnification (Figure 5-b) and with HAADF chemical contrast (Figure 5-a, c, d, e) showed differences in morphology, texture and composition between the gel and the pristine glass. Thus, the location of the interface

could be precisely determined. This piece of information is important to assess glass alteration with confidence.

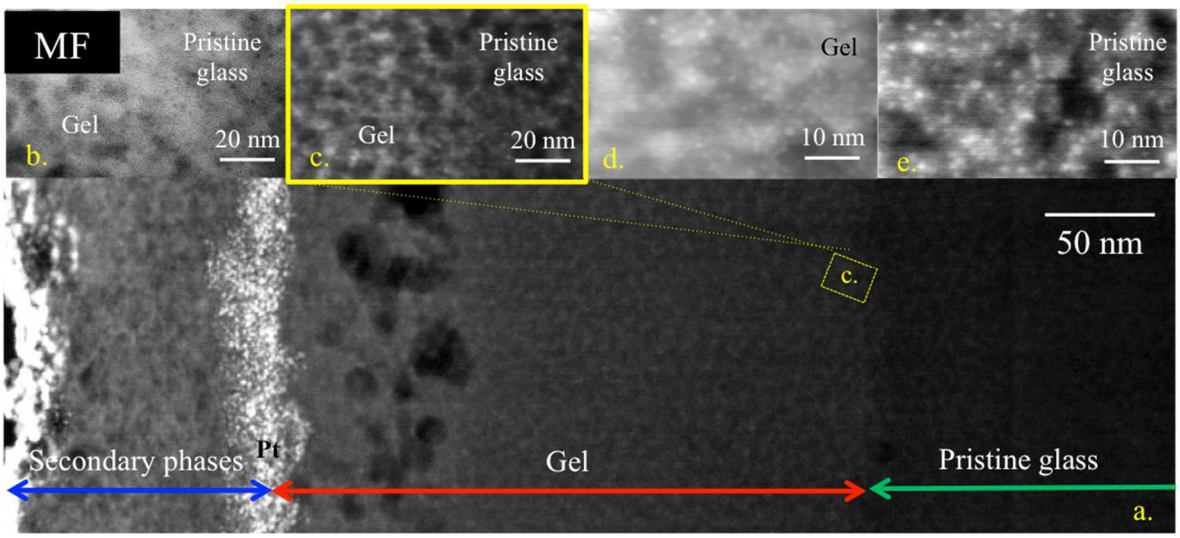

Figure 5: TEM observations of the gel / pristine glass interface of sample MF (ISG glass altered in the solution containing $MgCl_2$ and $FeCl_2$): HAADF (a, c, d, e) and HRTEM (b). TEM observations of the other samples are presented in SI 5.

.

Determination of the boron concentration profile

According to the procedure described before, the boron concentration profiles at the pristine glass / gel interface for altered glass samples F, CF and MF were studied by spatially-resolved EELS (Figure 6). In all cases, the boron concentration presented a S-shaped profile which could be fitted by a Boltzmann law. The thickness of the boron profile was close for F and MF samples (35 and 29 nm, respectively), and a slightly higher for CF sample (42 nm). This result suggests that the gel layer was more protective for CF sample than for F and MF ones, which is consistent with the results obtained in our previous work (Aréna, Rébiscoul et al. 2018). The thicknesses of the concentration profiles were much lower than those determined by ToF-SIMS analyses (273, 549 and 690 nm for samples MF, CF and F, respectively in SI 6). This can be explained by the presence of secondary phases at the sample surface forming irregularities and roughness which induce mixing areas and widen the boron profile at the interface when measured by ToF-SIMS (Gin, Jollivet et al. 2017). Therefore, EELS is a much better technique than ToF-SIMS for such non-planar samples when the objective is to describe precisely the feature of the alteration layer.

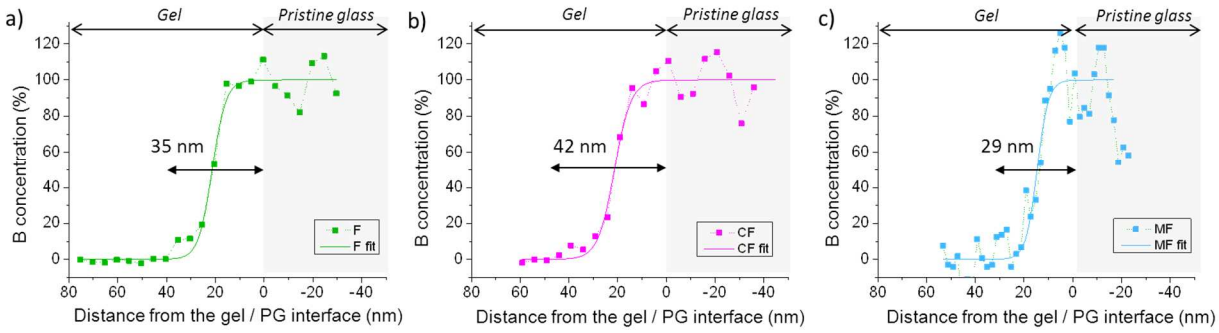

Figure 6: Boron profile at the pristine glass / gel interface, determined by EELS analyses for altered glass samples F, CF and MF. The position of the interface (x = 0), is defined for a boron concentration of 99.8 % on the fitted profiles. Positive x values are in the gel layer and negative x values are in the pristine glass area. The dot lines are the experimental data and the solid lines represent the fit obtained with a Boltzmann-type functions (SI 2). Black left right arrows show the thickness of the boron concentration profile determined by fitting (between 99.8 and 0.02% of B concentration). The error associated with the gradient thickness is about 7%, 8% and 10% for samples F, CF and MF, respectively.

Boron coordination along the profile

EEL spectra were acquired along the B concentration profile. For all three samples, a sharp decrease of the first peak (A) intensity was observed (Figure 7-a, b, c). In the case of sample F, the rising of a peak around 199 eV suggests an increase in the B^{IV} proportion. The evolution of the % B^{III} was calculated as long as the amount of boron detected was sufficient (Figure 7-d). Despite the increase in the error bars as the total concentration of B decreases when going deeper in the gel zone, a clear trend was observed: the % B^{III} decreased from the pristine glass to the gel, following the total boron concentration profile (Figure 6). Previous results about reference materials showed that B^{III} is more stable than B^{IV} under the electron beam. Therefore, the decrease in B^{III} proportion along the boron concentration profile cannot be an artefact due to electron beam irradiation, and is likely to be linked with glass alteration processes. In addition the relative evolutions of the integrated intensity of peak A and of peaks B+C (ΔE-A) along the profile were calculated to verify that the evolution was not an artefact due to the overall decrease in boron concentration (SI 7).

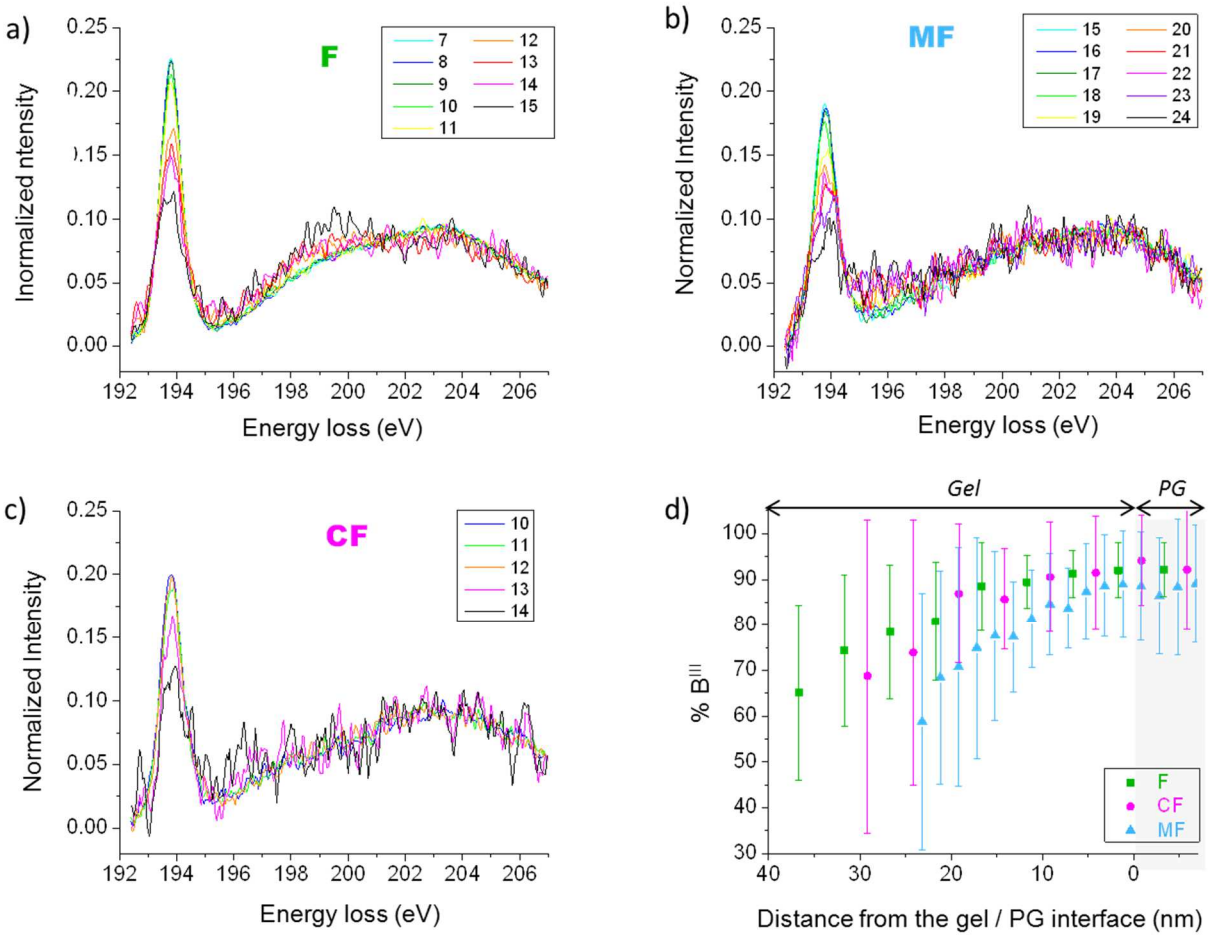

Figure 7: Evolution of the B EEL spectra (a, b, c) and of the B^{III} proportion (d) along the boron profile in the zone between the pristine glass and the gel. The calculation of the % B^{III} error is described in the SI 1.

Consequences for glass alteration study

The alteration of glass is generally described according to the following processes. During glass alteration, water penetration and ion exchange between the protons from the solution and the alkali from the glass weaken the Si – O – B bonds. This phenomenon favors two more or less simultaneous hydrolysis reactions (Geneste, Bouyer et al. 2006):

- the hydrolysis of 3 BO – T bonds (T being Si or B^{IV}) releases $B^{III}(OH)_3$ groups in the solution (Equation 3):

$$(TO)_3B^{III} + 3\ H_2O \longrightarrow B^{III}(OH)_3 + 3\ TOH \qquad (3)$$

- the hydrolysis of B – O bonds, transforms $B^{IV}(OT)_4$ groups into $B^{III}(OT)_3$ ones (Equation 4) which can then be released in solution following the Equation 3.

$$(TO)_3B^{IV} - OT + H_3O^+ \longrightarrow (TO)_3B^{III} + TOH + H_2O \qquad (4)$$

Because it is highly impossible for B^{III} to turn into B^{IV}, the decrease in the % B^{III} observed along the concentration profile could be explained by the faster decrease in the number of B^{III} units than that of B^{IV} ones. As a matter of fact, B can only be released in solution as $B^{III}(OH)_3$, thus the decrease in B overall concentration (evidenced by the presence of the B concentration decrease at the interface) would be mainly due to the release of $B(OH)_3$ units (after hydrolysis of B^{III}-OT bonds). However, there may be $B^{IV}(OT)_4$ groups turning into $B^{III}(OT)_3$ units and $B^{III}(OH)_3$ units being released in solution at the same time, thus, the % B^{III} depends on the initial proportion of B^{III} / B^{IV} in the pristine glass but also on the relative ability of $B^{IV}(OT)_4$ to be transformed into $B^{III}(OT)_3$ and of $B^{III}(OH)_3$ to be released.

Since glass alteration usually induces a basic pH, equation (4) is not favored. Nevertheless, this reaction occurs anyway since the concentration of boron into the gel layer is null. At some point, the $B^{IV}(OT)_4$ must be transformed into $B^{III}(OT)_3$, then into $B^{III}(OH)_3$ before being released into the solution. This transformation should induce an increase in the B^{III} percentage. So, it probably takes place at the left end of the profile, where the overall B concentration is too low to enable the interpretation of the EEL spectra. Therefore, these results suggest that the kinetic of transformation of $B^{III}(OT)_3$ groups into $B^{III}(OH)_3$ and their transport through the gel is faster than the transformation of $B^{IV}(OT)_4$ into $B^{III}(OT)_3$.

This finding is of primary importance in the assessment of nuclear waste glasses under repository conditions. Indeed, due to their composition, these materials are expected to endure irradiation from the high-level radioactive wastes they contain. Several studies reported higher glass alteration rates for irradiated glasses (Mougnaud, Tribet et al. 2018, Peuget, Tribet et al. 2018). Since electron beam exposure in TEM induces the transformation of B^{IV} into B^{III}, we can assume that self-irradiated glasses would contain more B^{III} units than non-irradiated ones. As we observed a faster release of B^{III} than the transformation of B^{IV}, a B^{III} rich glass would be altered more quickly. Based on this hypothesis, it would be interesting to compare the evolution of the boron coordination along the concentration profile in irradiated and non-irradiated altered glass samples.

3 Conclusions

In this study, the possibility to characterize the boron concentration profile in complex samples like altered glass layers at the nanometer scale using EELS coupled with HR-(S)TEM was demonstrated. The B concentration profile in the zone between the pristine glass and the gel, was found to be S-shaped with a thickness of about 40 nm.

From the local EEL spectra the speciation between trivalent and tetravalent boron was determined in mineral, pristine glasses, and for the first time, across the interface between the gel / pristine glass in altered glasses. The trivalent boron proportion was found to decrease along the boron concentration profile, indicating that the kinetic of B^{III} release in solution was favored compared to the transformation of B^{IV} into B^{III}. The determination of these profiles opens the possibility to a better description of the boron release from the pristine glass during the alteration process. Despite some difficulties to implement the method, the local description of the alteration layers, in terms of boron chemistry and speciation, that is reported herein, clearly evidence the importance to implement very local analytical spectroscopies associated to TEM to describe the glass alteration mechanisms.

4 Acknowledgments

This work was financed by AREVA, CEA and EDF. The authors acknowledge financial support from the CNRS-CEA “METSA” French network (FR CNRS 3507) (METSA 2015) for the aberration-corrected TEM experiments conducted on the MPQ (Université Paris Diderot) platform. Finally, we would like to thank Prime Verre *(Montpellier, France)* for glass monolith preparation.

5 Bibliography

References Cited

Aréna, H. (2016). Effets cumulatifs et compétitifs des éléments chimiques sur l'altération des verres nucléaires Ph-D thesis, Montpellier.

Aréna, H., N. Godon, D. Rébiscoul, R. Frugier, R. Podor, E. Garces, M. Cabie and J. P. Mestre (2017). "Impact of iron and magnesium on glass alteration: Characterization of the secondary phases and determination of their solubility constants." Applied Geochemistry **82**: 119-133.

Aréna, H., N. Godon, D. Rébiscoul, R. Podor, E. Garcès, M. Cabie and J. P. Mestre (2016). "Impact of Zn, Mg, Ni and Co elements on glass alteration: Additive effects." Journal of Nuclear Materials **470**: 55-67.

Aréna, H., D. Rébiscoul, E. Garces and N. Godon (2019). "Comparative effect of alkaline elements and calcium on alteration of International Simple Glass." npj Material Degradation **3**(10).

Aréna, H., D. Rébiscoul, R. Podor, E. Garcès, M. Cabié, J. P. Mestre and N. Godon (2018). "Impact of Fe, Mg and Ca elements on glass alteration: interconnected processes." Geochimica et Cosmochimica Acta **239**: 420-445.

Berger, S. D. and D. R. McKenzie (1988). "EELS analysis of vacuum arc-deposited diamond-like films." Philosophical Magazine Letters **57**(6): 285-290.

Bingham, P. A., G. Yang, R. J. Hand and G. Möbus (2008). "Boron environments and irradiation stability of iron borophosphate glasses analysed by EELS." Solid State Sciences **10**(9): 1194-1199.

Cailleteau, C., F. Angeli, F. Devreux, S. Gin, J. Jestin, P. Jollivet and O. Spalla (2008). "Insight into silicate-glass corrosion mechanisms." Nature Materials **7**(12): 978-983.

Chave, T., P. Frugier, S. Gin and A. Ayral (2011). "Glass-water interphase reactivity with calcium rich solutions." Geochimica and Cosmochimica Acta **75**(15): 4125-4139.

Cheng, S., G. Yang, Y. Zhao, M. Peng, J. Skibsted and Y. Yue (2015). "Quantification of the boron speciation in alkali borosilicate glasses by electron energy loss spectroscopy." Scientific Reports **5**: 17526.

Denatale, J. F. and D. G. Howitt (1984). "A mechanism for radiation damage in silicate glasses." Nuclear Instruments and Methods in Physics Research Bl **229**: 489.

Dillmann, P., S. Gin, D. Neff, L. Gentaz and D. Rebiscoul (2016). "Effect of natural and synthetic iron corrosion products on silicate glass alteration processes." Geochimica et Cosmochimica Acta **172**: 287-305.

Dubrovinskaia, N., R. Wirth, J. Wosnitza, T. Papageorgiou, H. F. Braun, N. Miyajima and L. Dubrovinsky (2008). "An insight into what superconducts in polycrystalline boron-doped diamonds based on investigations of microstructure." Proceedings of the National Academy of Sciences **105**(33): 11619-11622.

Duchamp, M., C. B. Boothroyd, M. S. Moreno, B. B. van Aken, W. J. Soppe and R. E. Dunin-Borkowski (2013). "Electron energy-loss spectroscopy of boron-doped layers in amorphous thin film silicon solar cells." Journal of Applied Physics **113**(9): 093513.

Fleury, B., N. Godon, A. Ayral and S. Gin (2013). "SON68 glass dissolution driven by magnesium silicate precipitation." Journal of Nuclear Materials **442**(1-3): 17-28.

Garvie, L. A. J., A. J. Craven and R. Brydson (1995). "Parallel electron energy-loss spectroscopy (PEELS) study of B in minerals; the electron energy-loss near-edge structure (ELNES) of the B K edge." American Mineralogist **80**: 1132-1144.

Geneste, G., F. Bouyer and S. Gin (2006). "Hydrogen-sodium interdiffusion in borosilicate glasses investigated from first principles." Journal of Non-Crystalline Solids **352**: 3147-3152.

Giannuzzi, L. A. and F. A. Stevie (1999). "A review of focused ion beam milling techniques for TEM specimen preparation." Micron **30**: 197-204.

Gin, S., A. Abdelouas, L. J. Criscenti, W. L. Ebert, K. Ferrand, T. Geisler, M. T. Harrison, Y. Inagaki, S. Mitsui, K. T. Mueller, J. C. Marra, C. G. Pantano, E. M. Pierce, J. V. Ryan, J. M. Schofield, C. I. Steefel and J. D. Vienna (2013). "An international initiative on long-term behavior of high-level nuclear waste glass." Materials Today **16**(6): 243-248.

Gin, S., C. Guittonneau, N. Godon, D. Neff, D. Rebiscoul, M. Cabié and S. Mostefaoui (2011). "Nuclear glass durability: new insight into alteration layer properties." The journal of Physical Chemistry C **115**(38): 18696-18706.

Gin, S., C. Guittonneau, N. Godon and D. Rebiscoul (2011). "Nuclear glass dissolution: new insight into alteration layer properties." soumis à Journal of Physical Chemistry C.

Gin, S., P. Jollivet, G. B. Rossa, M. Tribet, S. Mougnaud, M. Collin, M. Fournier, E. Cadel, M. Cabie and L. Dupuy (2017). "Atom-Probe Tomography, TEM and ToF-SIMS study of borosilicate glass alteration rim: A multiscale approach to investigating rate-limiting mechanisms." Geochimica Et Cosmochimica Acta **202**: 57-76.

Gin, S., P. Jollivet, M. Tribet, S. Peuget and S. Schuller (2017). "Radionuclides containment in nuclear glasses: an overview." Radiochimica Acta **105**(11): 927-959.

Gin, S., J. V. Ryan, D. K. Schreiber, J. Neeway and M. Cabie (2013). "Contribution of atom-probe tomography to a better understanding of glass alteration mechanisms: Application to a nuclear glass specimen altered 25 years in a granitic environment." Chemical Geology **349**: 99-109.

Hovden, R., P. Cueva, J. Miundy and D. Muller (2013). "The Open-Source Cornell Spectrum Imager." Microscopy today: 40 - 44.

Jiang, N. and J. Silcox (2004). "High-energy electron irradiation and B coordination in Na2O–B2O3–SiO2 glass." Journal of Non-Crystalline Solids **342**(1–3): 12-17.

K. Sun, L.M. Wang, R.C. Ewing and W. J. Weber (2004). "Electron irradiation induced phase separation in a sodium borosilicate glass." Nuclear Instruments and Methods in Physics Research B **218**: 368-374.

Lu, Y.-G., S. Turner, J. Verbeeck, S. D. Janssens, P. Wagner, K. Haenen and G. Van Tendeloo (2012). "Direct visualization of boron dopant distribution and coordination in individual chemical vapor deposition nanocrystalline B-doped diamond grains." Applied Physics Letters **101**(4): 041907.

Mansas, C., J. M. Delaye, T. Charpentier, F. Bruguier, O. Bouty, B. Penelon, H. Arena and D. Rebiscoul (2017). "Drivers of Water Transport in Glass: Chemical or Topological Effect of the Glass Network?" Journal of Physical Chemistry C **121**(30): 16201-16215.

Mendoza, C., S. Peuget, T. Charpentier, M. Moskura, R. Caraballo, O. Bouty, A. H. Mir, I. Monnet, C. Grygiel and C. Jegou (2014). "Oxide glass structure evolution under swift heavy ion irradiation." Nuclear Instruments and Methods in Physics Research Section B: Beam Interactions with Materials and Atoms **325**: 54-65.

Mercado-Depierre, S., F. Angeli, F. Frizon and S. Gin (2013). "Antagonist effects of calcium on borosilicate glass alteration." Journal of Nuclear Materials **441**(1-3): 402-410.

METSA (2015). "French network of facilities in electronic mircroscopy and atom probe."

Michelin, A., E. Burger, E. Leroy, E. Foy, D. Neff, K. Benzerara, P. Dillmann and S. Gin (2013). "Effect of iron metal and siderite on the durability of simulated archeological glassy material." Corrosion Science **76**: 403-414.

Mougnaud, S., M. Tribet, J.-P. Renault, S. Gin, S. Peuget, R. Podor and C. Jegou (2018). "Heavy ion radiation ageing impact on long-term glass alteration behavior." Journal of Nuclear Materials **510**: 168-177.

Moutanabbir, O., D. Isheim, D. N. Seidman, Y. Kawamura and K. M. Itoh (2011). "Ultraviolet-laser atom-probe tomographic three-dimensional atom-by-atom mapping of isotopically modulated Si nanoscopic layers." Applied Physics Letters **98**(1): 013111.

Peuget, S., M. Tribet, S. Mougnaud, S. Miro and C. Jégou (2018). "Radiations effects in ISG glass: from structural changes to long-term aqueous behavior." npj Material Degradation **2**(23).

Pring, A., V. K. Din, D. A. Jefferson and J. M. Thomas (1986). "The crystal chemistry of rhodizite: a re-examination." Mineralogical Magazine **50**: 163-172.

Ray L. Frost, Ricardo Scholz, Andrés Lopez, Yunfei Xi and Fernanda Maria Belotti (2013). "Infrared and Raman Spectroscopic Characterization of the Borate Mineral Vonsenite Fe2+ 2Fe3+BO5." Spectroscopy Letters: An International Journal for Rapid Communication.

Rébiscoul, D., J. Cambedouzou, I. Matar Briman, M. Cabié, H. P. Brau and O. Diat (2015). "Water Dynamics in Nanoporous Alteration Layer Coming from Glass Alteration: An Experimental Approach." The journal of Physical Chemistry C **119**(28): 15982-15993.

Rebiscoul, D., A. Van der Lee, F. Rieutord, F. Né, O. Spalla, A. El Mansouri, P. Frugier, A. Ayral and S. Gin (2004). "Morphological evolution of alteration layers formed during nuclear glass alteration : new evidence of a gel as a diffusive barrier;." Journal of Nuclear Materials **326**: 9-18.

Ricolleau, C., J. Nelayah, T. Oikawa, Y. Kohno, N. Braidy, G. Wang, F. Hue, L. Florea, V. Pierron Bohnes and D. Alloyeau (2013). "Performances of an 80–200 kV microscope employing a cold-FEG and an aberration-corrected objective lens." Microscopy **62**(2): 283-293.

Sauer, H., R. Brydson, P. N. Rowley, W. Engel and J. M. Thomas (1993). "Determination of coordinations and coordination-specific site occupancies by electron energy-loss spectroscopy: An investigation of boron—oxygen compounds." Ultramicroscopy **49**(1): 198-209.

Schneider, C. A., W. S. Rasband and K. W. Eliceiri (2012). "NIH Image to ImageJ: 25 years of image analysis." Nature Methods **9**(7): 671-675.

Shindou, E., N. Hamamura, A. Yoshida, Y. Kaburagi and Y. Hishiyama (2010). "An EELS study of an individual boron-doped multi-walled carbon nanotube." Carbon **48**(2): 572.

Turner, S., Y. Lu, H. Idrissi, S. D. Janssens, K. Haenen, A. F. Sartori, M. Schreck, J. Verbeeck and G. Van Tendeloo (2016). Local boron environment in B-doped diamond films studied by advanced TEM and spatially resolved EELS. Czechoslovak Microscopy Society, Czechoslovak Microscopy Society.

Turner, S., Y.-G. Lu, S. D. Janssens, F. Da Pieve, D. Lamoen, J. Verbeeck, K. Haenen, P. Wagner and G. Van Tendeloo (2012). "Local boron environment in B-doped nanocrystalline diamond films." Nanoscale **4**(19): 5960-5964.

Van Aken, B. B., M. Duchamp, C. B. Boothroyd, R. E. Dunin-Borkowski and W. J. Soppe (2012). "EELS measurements of boron concentration profiles in p-a-Si and nip a-Si solar cells." Journal of Non-Crystalline Solids **358**(17): 2179-2182.

Wang, Z., J. Liu, Y. Zhou, J. J. Neeway, D. K. Schreiber, J. V. Crum, J. V. Ryan, X.-L. Wang, F. Wang and Z. Zhu (2016). "Nanoscale imaging of Li and B in nuclear waste glass, a comparison of ToF-SIMS, NanoSIMS, and APT." Surface and Interface Analysis **48**(13): 1392-1401.

Wurzinger, P., P. Pongratz, P. Hartmann, R. Haubner and B. Lux (1997). "Investigation of the boron incorporation in polycrystalline CVD diamond films by TEM, EELS and Raman spectroscopy." Diamond and Related Materials **6**(5-7): 763-768.

Yang, G., G. Möbus, P. A. Bingham and R. J. Hand (2009). "Electron beam induced structure changes in borosilicate and borophosphate glasses: a comparison by energy loss spectroscopy." Physics and Chemistry of Glasses - European Journal of Glass Science and Technology Part B **50**(6): 378-383.

Yang, G., G. Mobus and R. J. Hand (2006). "EELS study of boron coordination in alkali borosilicate glasses under extensive electron irradiation." Physics and Chemistry of Glasses-European Journal of Glass Science and Technology Part B **47**(4): 507-512.

Yang, G., G. Möbus and R. J. Hand (2006). "Cerium and boron chemistry in doped borosilicate glasses examined by EELS." Micron **37**(5): 433-441.

Yang, G., Z. Saghi, X. Xu, R. Hand and G. Möbus (2007). EELS Spectrum Imaging and Tomography Studies of Simulated Nuclear Waste Glasses. Scientific Basis for Nuclear Waste Management XXX. D. Dunn, C. Poinssot and B. Begg. Boston, Massachussetts, USA, Materials Research Society**:** 187-192.